Received: 23 April 2023 | Revised: 13 June 2023 | Accepted: 6 July 2023

DOI: 10.1002/ar.25293

RESEARCH ARTICLE

The Anatomical Record WILEY

Anatomy of the female reproductive tract organs of the brown anole (*Anolis sagrei*)

Bonnie K. Kircher[1] | **Edward L. Stanley**[2] | **Richard R. Behringer**[1]

[1]Department of Genetics, University of Texas MD Anderson Cancer Center, Houston, Texas, USA

[2]Florida Museum of Natural History, University of Florida, Gainesville, Florida, USA

Correspondence
Richard R. Behringer, Department of Genetics, University of Texas MD Anderson Cancer Center, 1515 Holcombe Boulevard, Houston, TX 77030, USA.
Email: rrb@mdanderson.org

Funding information
National Institutes of Health, Grant/Award Numbers: HD30284, T32HD098068, OD024976, CA16672; National Science Foundation, Grant/Award Number: 2209150

Abstract

Female reproduction in squamate reptiles (lizards and snakes) is highly diverse and mode of reproduction, clutch size, and reproductive tract morphology all vary widely across this group of ~11,000 species. Recently, CRISPR genome editing techniques that require manipulation of the female reproductive anatomy have been developed in this group, making a more complete understanding of this anatomy essential. We describe the adult female reproductive anatomy of the model reptile the brown anole (*Anolis sagrei*). We show that the brown anole female reproductive tract has three distinct anterior-to-posterior regions, the infundibulum, the glandular uterus, and the nonglandular uterus. The infundibulum has a highly ciliated epithelial lip, a region where the epithelium is inverted so that cilia are present on the inside and outside of the tube. The glandular uterus has epithelial ducts that are patent with a lumen as well as acinar structures with a lumen. The nonglandular uterus has a heterogeneous morphology from anterior to posterior, with a highly folded, ciliated epithelium transitioning to a stratified squamous epithelium. This transition is accompanied by a loss of keratin-8 expression and together, these changes are similar to the morphological and gene expression changes that occur in the mammalian cervix. We recommend that description of the nonglandular uterus include the regional sub-specification of a "cervix" and "vagina" as this terminology change more accurately describes the morphology. Our data extend histological studies of reproductive organ morphology in reptiles and expand our understanding of the variation in reproductive system anatomy across squamates and vertebrates.

KEYWORDS

infundibulum, ovary, oviduct, uterus

1 | INTRODUCTION

Squamate (lizards and snakes) reproductive strategies are strikingly diverse when compared to the conserved reproductive modes of the other amniote lineages (mammals, birds, crocodiles, turtles, and tuataras). Squamates account for all but one of the 115 independent origins of viviparity in amniotes (Blackburn, 1999), with some species having such high reproductive plasticity that their reproductive mode varies across their geographic ranges (reviewed in Tinkle & Gibbons, 1977). Within the derived viviparous forms, both lecithotrophic (embryonic nutrients come from yolk) and matrotrophic (embryonic nutrients come from mother) viviparity have been

documented (reviewed in Blackburn, 2015). Clutch size also varies between species with lizards producing from one to 21 (viviparous)/52 (oviparous) offspring at a time across the breeding season (Meiri et al., 2020). Despite this diversity of reproductive mode and clutch size, the gross anatomy of the lizard female reproductive tract appears to be more conserved (Blackburn, 1998; Girling, 2002) than that of eutherian mammals (Machado et al., 2022). However, a comprehensive understanding of the morphological diversity in the reproductive organs of squamates is lacking and many groups of reptiles remain understudied.

The generalized squamate reptile female reproductive tract is composed of paired tubes located at the dorsal side of the coelomic cavity, opening anteriorly to the ovary and connecting posteriorly with the gastrointestinal system in a single opening called the cloaca. In adult females, the reproductive tracts are heterogeneous and have morphologically distinct regions. The infundibulum is the most anterior region and is a thin, folded tube that receives the ovulated oocyte from the ovary (Bassi et al., 2018; Cuellar, 1970). The infundibulum transitions into the glandular uterus, a region with a thicker epithelium and a large portion of glandular tissue where the fertilized eggs are maintained during the initial stages of embryogenesis (reviewed in Blackburn, 1998). More posteriorly, the glandular uterus transitions into the nonglandular uterus, a muscular organ that has been described as the location of sperm storage in some species (Conner & Crews, 1980, reviewed in Sever & Hamlett, 2002). The nonglandular uterus connects to the cloaca. This same general architecture is consistent between lecithotrophic viviparous (ovoviviparous; Girling et al., 1997; Murphy et al., 2011) and oviparous species (Blackburn, 1998; Siegel et al., 2014). Though we were unable to find descriptions of the full length of the reproductive tract in a matrotrophic viviparous (placental) species, the uterine region in these species has been similarly described (Adams et al., 2007; Biazik et al., 2008, 2009; Parker et al., 2010; Thompson et al., 2006; Wu et al., 2011).

Morphological and functional studies of the female reproductive tract organs of nonavian reptiles have given rise to a set of terminology that has been used to describe the adult reproductive anatomy of the female reproductive tract. As early as 1893, the central portion of the female reproductive tract was named the "uterus" as this is the region of the reproductive tract where fertilized eggs spend most of their time. The reptilian "uterus" is morphologically defined by two layers of muscle, the presence of mucosal glands, and the presence of ciliated and secretory cells (Siegel et al., 2014). From 1898 onwards, the posterior region of the reproductive tract was named the "vagina" and this region was defined morphologically by a thick muscle layer, highly folded mucosa, and ciliated crypts where sperm is stored in some species (Siegel et al., 2014). Despite the persistent use of these terms in studies of the reptilian reproductive anatomy, the homology of these regions to the synonymous regions of the mammalian and avian reproductive tracts have not been assessed. Some recent studies replace the term "uterus" with the term "glandular uterus" and the term "vagina" with the term "nonglandular uterus" (Siegel et al., 2014). The most anterior portion of the reproductive tract, often named the infundibulum, is also referenced as the uterine tube (Adams et al., 2004) but this terminology is less common. The infundibulum is defined by the presence of both ciliated and nonciliated cells (Siegel et al., 2014). Additionally, some but not all descriptions of the reproductive anatomy across reptiles include additional morphological distinctions between regions of the reproductive tract. A region described as an isthmus has been reported between the infundibulum and the glandular uterus, primarily in geckos (Girling, 2002; Girling et al., 1997, 2000; Nogueira et al., 2011) but there is no broad use of this term and regional distinction. Thus, because of incomplete histological analyses, unique naming conventions, and varied interpretations, morphological distinctions within the literature are challenging to interpret (Blackburn, 1998). In this article, we use the terminology that describes three regions of the reproductive tract: the infundibulum, the glandular uterus, and the nonglandular uterus.

Relatively few studies of the reproductive system have focused on Iguania, a morphologically and ecologically diverse superfamily comprising 20% of all squamate species (27% of all lizards). The lizard genus *Anolis* is a diverse group of Iguanian lizards that has long been a focus of research on convergent evolution, ecological adaptation, behavior, biogeography, and morphological variation (Losos, 2009). The brown anole, *Anolis sagrei*, has become an important species due to being readily adaptable to laboratory conditions, the accessibility of the lizards, and the availability of tools for study (Geneva et al., 2022; Lovern et al., 2004; Sanger & Kircher, 2017). Study of this species is particularly important as technological advances in genome editing that rely heavily on manipulation of the reproductive tract have been recently developed (Abe et al., 2023; Garcia-Elfring et al., 2023; Rasys et al., 2019). The adult female reproductive anatomy of the genus *Anolis* has been described as highly conserved and follows a generalized reptilian architecture (Conner & Crews, 1980; Evans & Clapp, 1940; Fox, 1963; Fox & Dessauer, 1962; Gabe & Saint Girons, 1965; Ortiz & Morales, 1974; Sever & Hamlett, 2002). Although most of these studies do not

focus on morphological distinctions between the regions of the reproductive tract, Noble & Greenberg (1941) outline distinctions between the glandular and nonglandular uterus in the green anole *Anolis carolinensis*. The green anole glandular uterus has acinar glands that appear to be associated with epithelial folds. The nonglandular uterus has three lumen that merge into one and an epithelium that changes from cuboidal/columnar, to multilayered from anterior to posterior. Throughout the breeding season, female anoles lay approximately one egg per week, and ovulation alternates between left and right ovaries (reported in the green anole; Crews, 1977, 1980). Sperm storage in the nonglandular uterus has been described in *Anolis sagrei* (Sever & Hamlett, 2002). However, study of the entire reproductive anatomy of the brown anole is less comprehensive.

Here, we describe the morphology of the reproductive tract of the adult female brown anole and employ histological and molecular characterization to define distinct subregions along the anterior–posterior axis. We examine the expression of genes known to be present in the mammalian and avian reproductive tracts. Specifically, we use antibodies against keratin 8, a gene that is expressed in the anterior portions of the mammalian reproductive tract (uterus, oviduct) but absent from posterior portions (vagina; Chumduri et al., 2021) and laminin, a gene that is expressed in the basement membranes surrounding ducts in the avian shell gland (Madekurozwa, 2013). We also use general gene expression markers of smooth muscle (smooth muscle actin) and cilia (beta-tubulin) for a more detailed study of the tissue architecture across the brown anole reproductive tract. These detailed studies provide a foundation for future investigations of reproductive biology and development in this important reptilian species.

2 | MATERIALS AND METHODS

2.1 | Lizards

Adult and subadult *Anolis sagrei* were collected at the University of Florida (Gainesville) in August 2017 under University of Florida IACUC protocol #201809270 (Martin Cohn, PI) and from the Houston Arboretum and Nature Center between October 2021 and August 2022. Adult lizards collected in Houston were housed according to laboratory husbandry protocols for this genus (Sanger et al., 2008). The animals were supplied with water by daily misting, fed crickets dusted with a calcium supplement (Repta Calcium, Flukers) at least twice per week, and maintained on a 13:11 hour light:dark cycle (UVA/UVB light, Reptisun, ZooMed). Lizards were anesthetized by intracelomic injection of 1% buffered tricaine methanesulfonate based on body weight and euthanized with an intracelomic injection of 50% tricaine methanesulfonate based on body weight (Conroy et al., 2009; MD Anderson IACUC protocol) or euthanized by an intraperitoneal injection of Euthasol (UF IACUC protocol). The Institutional Animal Care and Use Committee of the University of Florida and the University of Texas MD Anderson Cancer Center approved all animal procedures. Experiments were performed consistent with the National Institutes of Health Guidelines for the Care and Use of Experimental Animals.

2.2 | Histology

The reproductive tracts from female lizards were dissected into phosphate-buffered saline. The freshly dissected tracts were then imaged using a Leica MZ10F dissecting microscope with a Jenoptik Gryphax camera. Tissues were subsequently fixed in 4% paraformaldehyde at 4°C overnight. Samples were then processed for paraffin embedding and 5 μM transverse sections were cut. Tissues were stained with hematoxylin and eosin (H&E) following standard procedures. H&E-stained sections were imaged using a Nikon Eclipse 80i compound microscope.

2.3 | Immunofluorescent staining

Fluorescent immunohistochemistry was performed on 5 μM paraffin sections to localize Keratin 8 (TROMA-1, Developmental Studies Hybridoma Bank, diluted to 3 μg/mL), Smooth Muscle Actin (SMA 546, Sigma, C6198, 1:200), Laminin (Sigma-Aldrich, L9393, 1:100), and beta-Tubulin (D3ULW, 1:400, Cell Signaling Technologies, 86298). After paraffin sections were dewaxed and rehydrated, antigen retrieval using a citrate buffer (10 mM citratric acid with 0.5% Tween, pH 6.0) and a 2100 Antigen Retriever (Aptum Biologics Ltd, South Hampton, UK) was performed. Samples were blocked using 5% fetal bovine serum (FBS) and primary antibodies were incubated overnight at 4°C. Fluorophore-conjugated secondary antibodies (goat anti-Rat Alexa-Fluor-488, Invitrogen, A-11006 or goat anti-Rabbit Alexa-Fluor-488, Invitrogen, A-11008) were added for 1 h at room temperature, and DAPI (1 mg/mL) for 5 min. #1.5 coverslips were mounted using Prolong Gold Antifade Mounting Media (Invitrogen, P36930). Fluorescent images were acquired with an A1 Nikon Inverted confocal equipped with a LUNV Laser Launch (405/445/488/514/561/640) and DU-G GaAsP detector

unit. Images were acquired using either a Plan Apo 20× 0.75 NA objective or an oil immersion Plan-Apo 60× 1.4 NA. Excitations were done with 405, 488, 561, and 640 nm laser lines, and respective emissions were collected with filters 450/50 (blue), 525/50 (green), 600/50 (red), and 650LP (far-red). The dwell time for each channel was 2.2 s/frame. Pinhole was set to be 1. The pixel size was 621.48 nm for 20× and 207.16 nm for 60×. Z-stack steps are reported in figure legends. A montage was made of X by Y tiles using an overlap of 15%. 3D rendering was performed using Fiji (Schindelin et al., 2012).

2.4 | Whole-mount immunofluorescent staining

Tissue was fixed in 4% paraformaldehyde overnight at 4°C then blocked with 5% FBS and 0.4% Triton-X 100 in phosphate-buffered saline. Primary antibodies against beta-Tubulin (D3ULW, 1:400, Cell Signaling Technologies, 86298), Laminin (Sigma-Aldrich, L9393, 1:100), or Keratin-8 (TROMA-1, Developmental Studies Hybridoma Bank, diluted to 3 µg/mL) and a secondary antibody (goat anti-Mouse Alexa-Fluor-546, A-11030, goat anti-Rabbit Alexa Fluor-546, A-11035, goat anti-Rat Alexa Fluor-488, A-11006, Invitrogen) were used. Tissue was cleared in ScaleS (Hama et al., 2015) for 48 h and mounted for imaging in ScaleS with a #1.5 coverslip. Fluorescent images were acquired using an A1 Nikon Inverted confocal microscope equipped with a LUNV Laser Launch (405/445/488/514/561/640) and DU-G GaASP detector unit. Images were acquired using a Plan Apo 10× 0.45 NA objective. Excitations were done with 405 and 561 nm lasers and respective emissions were collected with filters 450/50 (blue) and 600/50 (red). The dwell time for each channel was 2.2 s/frame. Pinhole was set at 1. The pixel size was 1.24 µm. A montage was generated of X by Y tiles using an overlap of 15% for the infundibulum. Deconvolution of the images of the infundibulum was performed using NIS Elements and the final image was rendered as an Extended Depth of Focus (EDF) image. A tiff stack of the glandular uterus data was processed in Fiji (Schindelin et al., 2012).

2.5 | Micro-computed tomography

Two formalin-fixed, ethanol-preserved female anoles were stained with contrasting agents, and their reproductive tract was visualized with high-resolution X-ray computed tomography. One subadult specimen was stained using a 1.75% aqueous solution of Lugol's iodine, following the guidelines for diffusible iodine-based contrast-enhanced CT (diceCT) from Gignac et al. (2016). The second adult specimen was stained with a 1.25% solution of phosphotungstic acid (PTA), following the removal of its integument, to allow for better diffusion, after the method of Lesciotto et al. (2020). Both samples were scanned on an Xradia Versa 620 system at the University of Florida's Nanoscale Research Facility. A lower-resolution (voxel size diceCT = 11.843 µm PTA = 19.352 µm) scouting scan was performed on the specimen's abdomen to locate the coordinates of the nonglandular uterus, then high-resolution (voxel size diceCT = 1.78 µm PTA = 1.09 µm) scans were performed using a 4× objective. Source and detector settings were modified to optimize signal-to-noise while still retaining a scan time that would minimize specimen movement (Table S1). Radiographs were converted to tomograms using the Scout and scan control system Reconstructor software v.16.0.11592 (Carl Zeiss Microscopy, GmbH), and postprocessing segmentation and visualization were performed with VGStudioMax 2022.4.1 (Volume Graphics, Heidelberg, Germany). Both scans are available to be viewed and downloaded on Morphosource.org.

3 | RESULTS

3.1 | Brown anole female reproductive tract organs

To determine whether female reproductive organ anatomy in *A. sagrei* is similar to other reptilian species, we examined the adult female reproductive tract in whole mount. We report that the female *A. sagrei* reproductive organ system is made up of paired ovaries that are located adjacent to paired reproductive tracts comprised of an infundibulum, glandular uterus, and nonglandular uterus that meet the digestive tract at the cloaca. (Figure 1a,b). In the nonbreeding season (~November–March in Houston, TX), the ovaries are smaller overall, the largest ovarian follicles have little to no yolk deposited, and there are rarely fertilized eggs in the reproductive tract (Figure 1a). In the breeding season, the ovaries are larger as the most mature ovarian follicles nearing ovulation have a large amount of yolk deposited (Figure 1b). A female usually carries 0–2 fertilized eggs but typically only one fertilized egg is present in each reproductive tract at a given time (Figure 1b).

To better understand the morphological variation along the anterior–posterior axis of the reproductive tract, we used histology to characterize the changes in cellular architecture across the reproductive tract regions. We also examined the spatial expression of the proteins

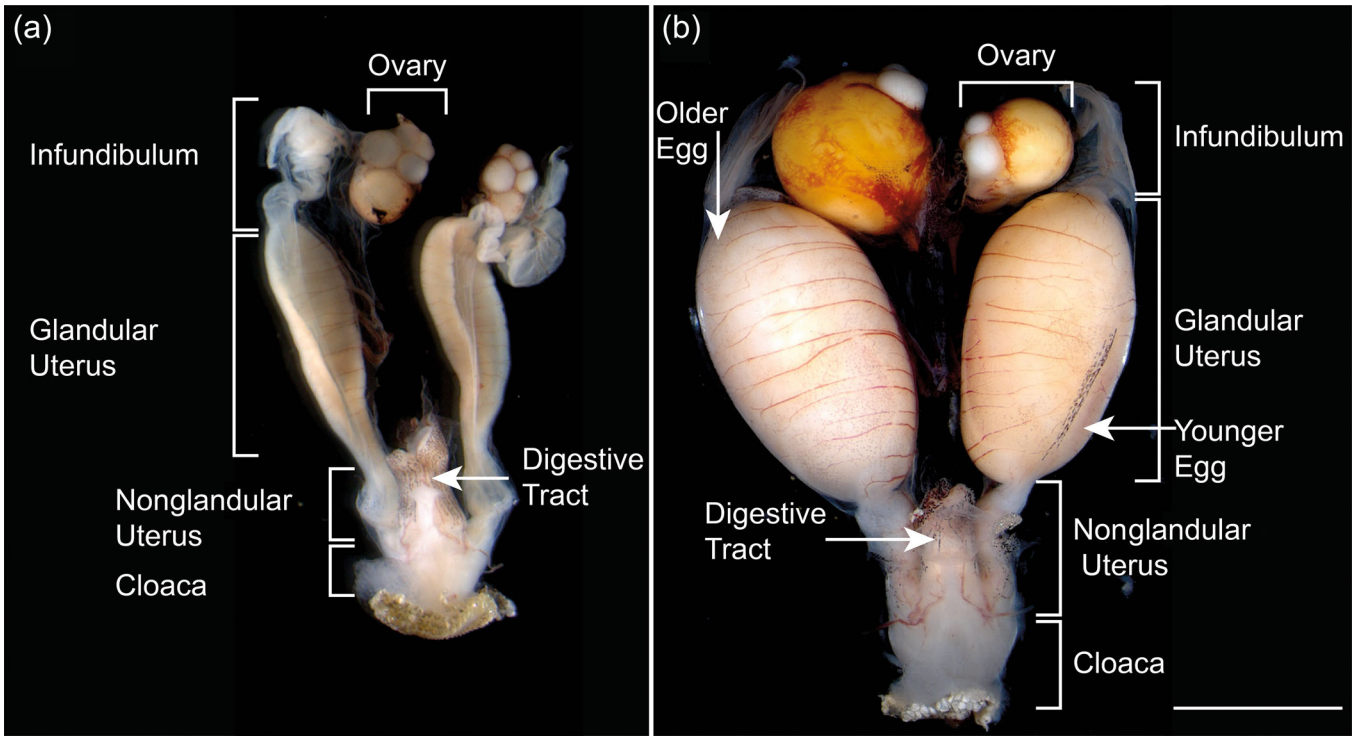

FIGURE 1 Ventral views of the adult brown anole female reproductive tracts. (a) During the nonbreeding season, there are no yolk-laden follicles. No eggs are found in the oviducts. (b) During the breeding, there are large, yolk-laden follicles present in each oviduct. The older (largest) egg will be laid first, as the younger (smaller) egg on the contralateral side continues to grow. Similarly, the largest ovarian follicle will be ovulated first while the largest on the contralateral side continues to grow. Scale bar = 5 mm.

smooth muscle actin (SMA), a marker of smooth muscle, keratin 8 (TROMA-1), an epithelial marker, beta-tubulin, a marker of cilia, and laminin, a basement membrane marker.

3.2 | Infundibulum

The infundibulum in *A. sagrei* is a thin, pliable, funnel-shaped tube (Figure 2a). It is composed of a simple cuboidal/columnar epithelium that is irregularly folded and a thin layer of smooth muscle (Figure 2a). The cuboidal/columnar epithelium of the posterior infundibulum consists of both ciliated and nonciliated cells (Figure 2b,c). In the posterior infundibulum, ciliated and nonciliated cells are interspersed, and the ciliated cells are recessed so that the cilia reach the same height as the neighboring nonciliated cells (Figure 2b). The cilia are beta-tubulin positive, and the ciliated cells are keratin 8 positive while nonciliated cells are keratin 8 negative (Figure 2c). The anterior opening of the infundibulum, the funnel, has a unique morphology compared to the posterior infundibulum. The most anterior epithelium of the infundibulum has a structure we define as the "funnel lip"; the funnel lip has an opaque, ribbon-like appearance in whole-mount (Figure 3a). In cross-section, the epithelium of the funnel lip is observed to be folded back onto itself and every cell of the funnel lip is ciliated. Because the epithelium is folded back on itself, cilia are present on the lumen facing or "inside" and coelom facing or "outside" of the funnel lip (Figure 3b). We find that in whole-mount and in section, the cilia of the infundibulum funnel lip are beta-tubulin positive, present in a ribbon across the most anterior region of the infundibulum (Figure 3c) and present on the inside and outside of the infundibulum funnel (Figure 3d).

In the posterior infundibulum, the cuboidal/columnar epithelium has interspersed keratin 8 positive and keratin 8 negative cells (Figure 4a,a′,d,d′). All observable muscle in the infundibulum expresses smooth muscle actin (Figure 4b,b′,d,d′).

3.3 | Glandular uterus

The glandular uterus is a thicker tube that, without a fertilized egg, is collapsed so that it appears flat. With a fertilized egg, the glandular uterus is transparent and stretched entirely around the developing eggshell. It is lined by a simple cuboidal epithelium with a glandular

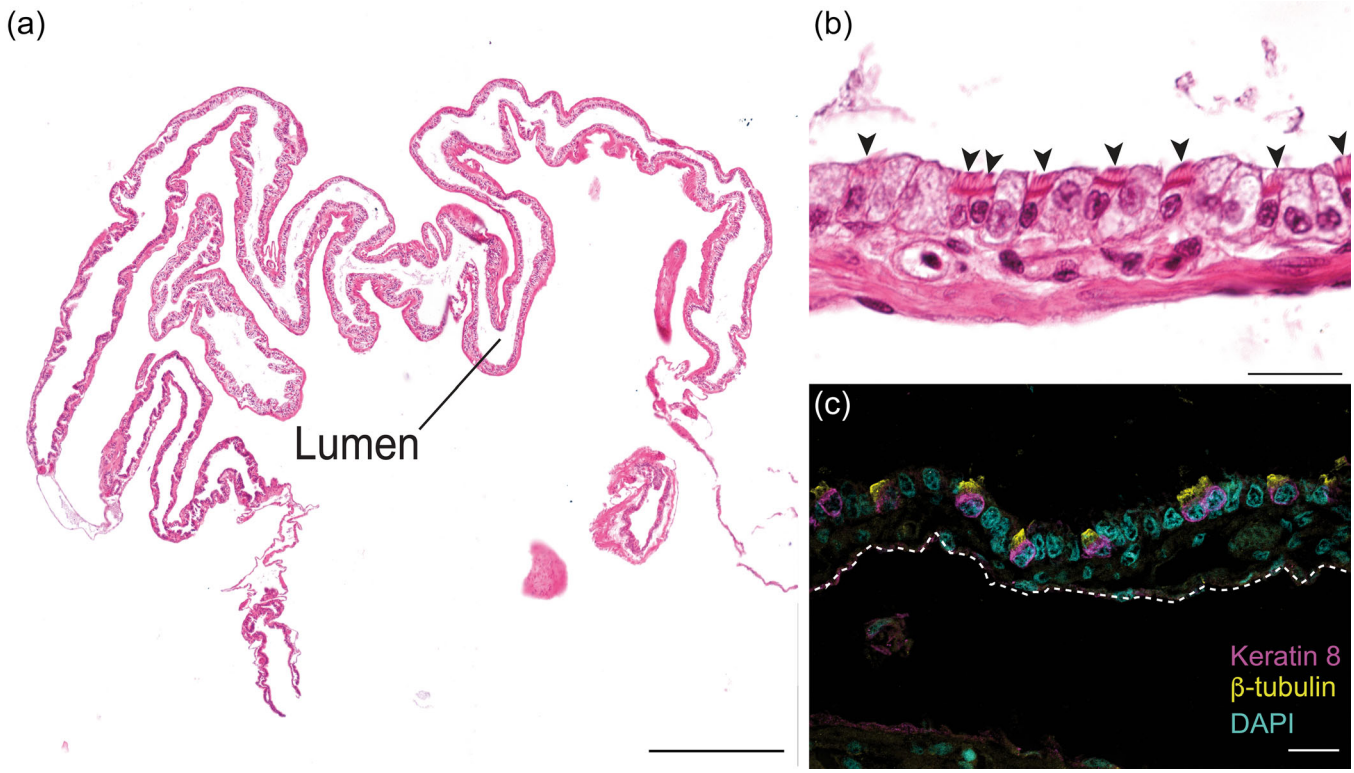

FIGURE 2 (a) Transverse cross-section of the posterior infundibulum, midway through the length of the organ. Scale bar = 500 μm. $n = 3$. (b) High-magnification image of a posterior infundibulum transverse cross-sections. Black arrowheads indicate ciliated cuboidal epithelial cells. Scale bar = 20 μm. $n = 3$. (c) High-magnification image of keratin 8 (magenta), beta-tubulin (yellow), and DAPI (cyan) immunofluorescence staining of a posterior infundibulum transverse cross-section. Scale bar = 20 μm. $n = 3$. In high-magnification images (b, c), lumen is on the top of the image.

layer surrounded by a smooth muscle layer (Figure 5a). The inner layer of muscle is circular around the glandular uterus as we primarily see longitudinal muscle fibers in cross-section while the outer layer of muscle is longitudinal as we see circular muscle fibers in cross-section. (Figure 5b). The middle tissue layer of the glandular uterus is made up of groups of cells organized into acinar structures with a lumen and a surrounding basement membrane (Figure 5c). The acinar structures of the glandular layer seen in H&E histology are surrounded by a laminin positive basement membrane (Figure 5d). We also observe epithelial duct-like projections within the glandular region that are patent with a lumen (Figure 5e). The epithelium of the glandular uterus has a simple cuboidal morphology (Figure 5e), and cilia are present on some of the epithelial cells (Figure 5f).

The epithelium of the glandular uterus is keratin 8 positive (Figure 6a,a′,d,d′). In the glandular uterus, the duct-like projections that extend into the uterine tissue from the epithelium are keratin 8 positive (Figure 6a,a′,d,d′). The glandular uterus also has two muscle layers in the glandular uterus that are SMA positive, one longitudinal and one circular (Figure 6bb′,d,d′).

In whole-mount, the keratin 8 positive epithelial protrusions appear to be associated with the network of laminin-positive basement membrane ductal structures (Video 1).

3.4 | Nonglandular uterus

The nonglandular uterus is a short, highly muscular tube that connects the glandular uterus to the cloaca. It has a heterogeneous morphology from anterior to posterior. Most anteriorly, immediately posterior to the glandular uterus, the lumen of the nonglandular uterus is lined by a simple cuboidal epithelium that is ciliated and extensively folded (Figure 7a,a′). We find that this region of the nonglandular uterus has sperm stored in small, isolated lumens surrounding the central lumen (Figure 7a″). In the middle region of the nonglandular uterus, the lumen narrows, and two additional lumens are present on each side (Figure 7b). The central lumen is surrounded by a simple columnar, ciliated epithelium (Figure 7b′), and the two lateral lumens are surrounded by nonciliated epithelial cells (Figure 7b″). More

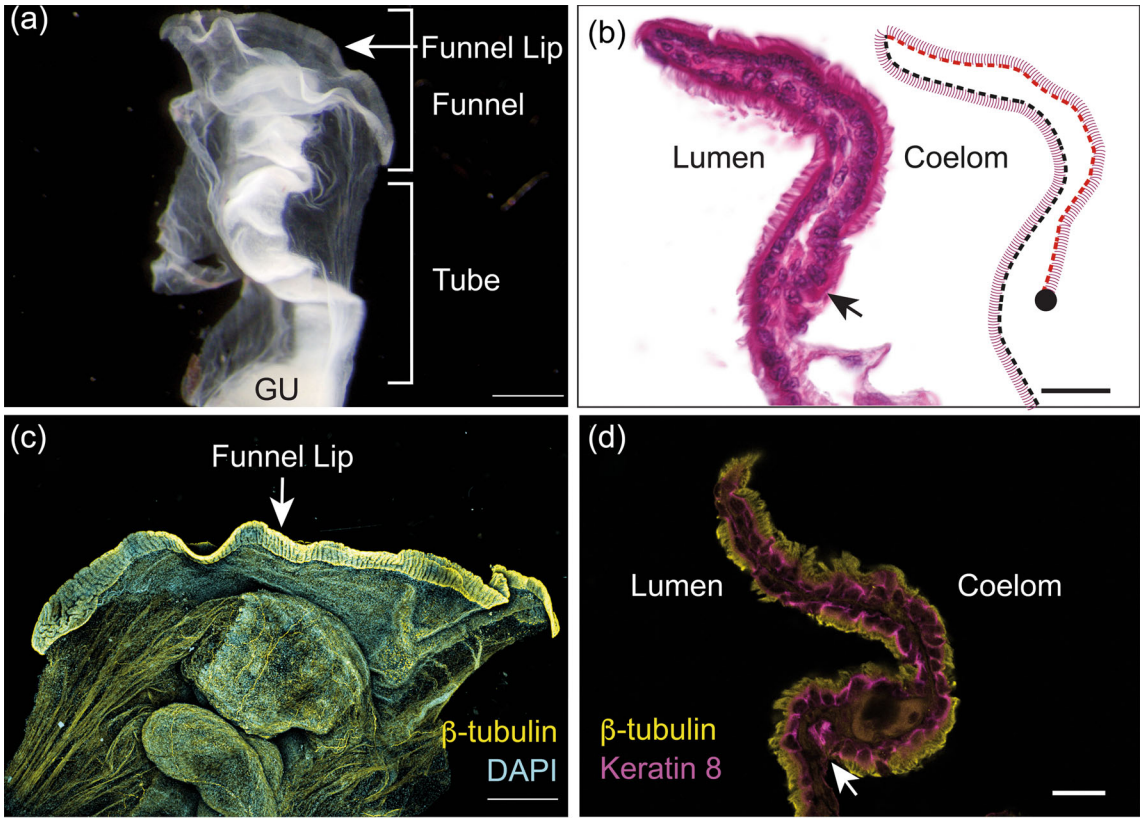

FIGURE 3 (a) Ventral view of the infundibulum dissected away from the rest of the reproductive tract. Scale bar = 2 mm. $n = 3$. GU = glandular uterus. (b) Cross-section of the funnel lip of the infundibulum. Black arrow indicates where the folded epithelium with coelom facing (exterior) cilia ends. Dashed line is a schematic representing how the connective tissue of the epithelium is doubled over at the funnel lip (black dashes represent epithelium with cilia facing the lumen, red dashes represent epithelium with cilia facing the coelom); the magenta lines represent the cilia from the cells of the epithelium of the infundibulum lip. $n = 3$. Scale bar = 20 μm. (c) Whole-mount image of beta-tubulin (yellow) and DAPI (cyan) expression in the infundibulum. 3.9 μm Z-step, 762.45 μm total thickness, $n = 3$. Scale bar = 500 μm. (d) Cross-section of the funnel lip of the infundibulum with beta-tubulin (yellow) and keratin 8 (magenta) staining. White arrowhead indicates where the folded epithelium with exterior cilia ends. $n = 3$. No Z-step. Scale bar = 20 μm.

posteriorly, there is a single lumen in a "W" shape (Figure 7c). The epithelium is columnar; however, there is a transition from ciliated to nonciliated cells (Figure 7c′). The central epithelial invagination is heavily ciliated (Figure 7c″) while the remaining epithelium is nonciliated. In the posterior region of the nonglandular uterus, the nonstratified, nonciliated columnar epithelium transitions to a squamous stratified epithelium (Figure 7d,d′,d″). The most posterior nonglandular uterus has a uniform stratified squamous epithelium (Figure 7e,e′). All the nonglandular uterus is surrounded by a large ring of smooth muscle and smooth muscle separates the three lumens in the anterior nonglandular uterus. The smooth muscle primarily runs circularly around the nonglandular uterus as the fibers are longitudinal in cross-section (Figure 7a–e).

The epithelium of the anterior nonglandular uterus is keratin 8 positive (Figure 8a,d). In the middle portion of the nonglandular uterus, the columnar, ciliated epithelium lining the central lumen is keratin 8 positive; similarly, the anterior portion of the columnar, nonciliated epithelium lining the two lateral lumens is keratin 8 positive (Figure 8e,h). The more posterior portions of the columnar, nonciliated epithelium lining the lateral lumen are keratin 8 negative (Figure 8i,l) and the stratified squamous epithelium of the most posterior region of the nonglandular uterus is keratin 8 negative (Figure 8m,p). All the observable muscle in the nonglandular uterus is smooth muscle actin positive (Figure 8b, f, j, n).

To better understand the gene expression changes from anterior to posterior across the epithelium of the nonglandular uterus, we collected coronal sections of the nonglandular uterus and stained for expression of keratin 8. As observed in transverse sections, the central lumen of the nonglandular uterus becomes keratin 8 positive when the lateral lumen separates and remains keratin 8 positive through the rest of the reproductive tract

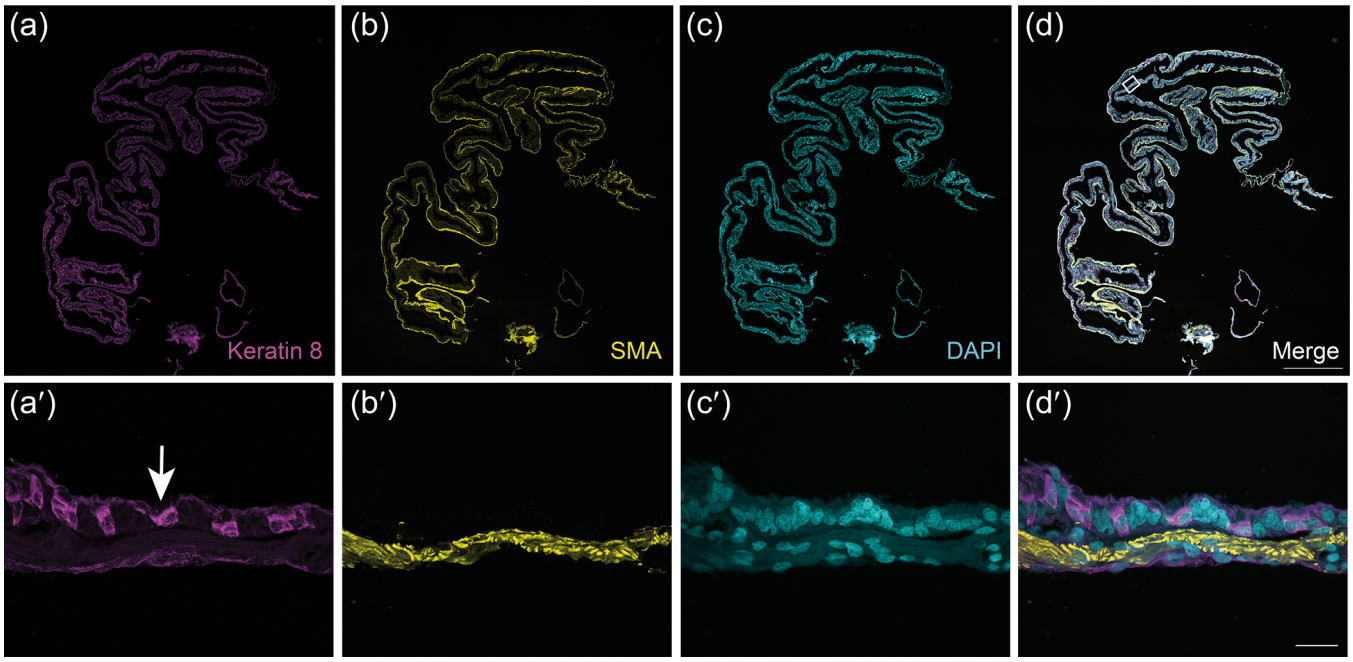

FIGURE 4 Immunohistochemistry of transverse sections of the posterior infundibulum. (a, a′) Keratin 8 (magenta), (b, b′) smooth muscle actin (yellow), (c, c′) DAPI (cyan), and (d, d′) merged composite antibody staining is shown. a–d scale bar = 500 μm, tiled images, a′–d′ scale bar = 20 μm, $n = 3$. Z-step = 2.4 μm, total depth = 12 μm for a–d and Z-step = 0.68 μm, total depth = 10.2 μm for a′–d′. In high-magnification images (a′–d′), lumen is on the top of the image. Box showing where magnified images were collected are approximate as magnified images were collected from different serial sections.

(anterior nonglandular uterus, glandular uterus, and infundibulum; Figure 9a). To characterize the three-dimensional structure of the nonglandular uterus, we digitally isolated the lumen from a microCT scan. The three-dimensional micro-CT segmentations reveal that the lumen has a series of internal folds to produce an intramural junction where the tube of the nonglandular uterus folds in on itself (Videos 2–4). At this junction, the anterior, ciliated epithelium becomes laterally compressed and angled medioventrally before meeting the posterior unciliated epithelium. The posterior, nonciliated epithelium is folded over on itself (inverted) to form a bowl (cupula), the sides of which extend anteriorly, bracketing the ciliated epithelium (Videos 2–4). At this junction where the anterior, ciliated epithelium meets the posterior, nonciliated epithelium, the anterior lumen is almost completely closed. The closed lumen and the angle of this junction form a kinked barrier between the anterior and posterior nonglandular uterus (Figure 9b, Videos 2–4).

4 | DISCUSSION

Reptile reproduction is diverse and understudied. Recent advances in genome modification in *A. sagrei* rely heavily on manipulation of the reproductive system, and a deeper understanding of the reproductive tract in this species will facilitate the continued development of genetic tools. In this study, we show that the *A. sagrei* reproductive tract has three distinct morphological regions as described in other reptilian species including an infundibulum, a glandular uterus, and a nonglandular uterus (reviewed in Blackburn, 1998; Siegel et al., 2014). We describe spatial patterns of gene expression throughout the reproductive tract, use three-dimensional imaging techniques to more completely describe the morphology of the infundibulum and the nonglandular uterus, and recommend a revision to naming conventions in the nonglandular uterus (Figure 10).

4.1 | Infundibulum

Using whole-mount antibody staining, we have identified a highly ciliated funnel lip on the infundibulum of the brown anole. The epithelium of the funnel lip is a simple columnar epithelium in which every cell is ciliated. This epithelium folds over on itself so that the cilia coat the exterior and interior of the anterior infundibulum. Posteriorly, the infundibulum epithelium has interspersed ciliated and nonciliated cells. These nonciliated cells are likely secretory cells, as have been described in snakes (Rojas et al., 2019) and in mammals (Crow et al., 1994). Although we have not

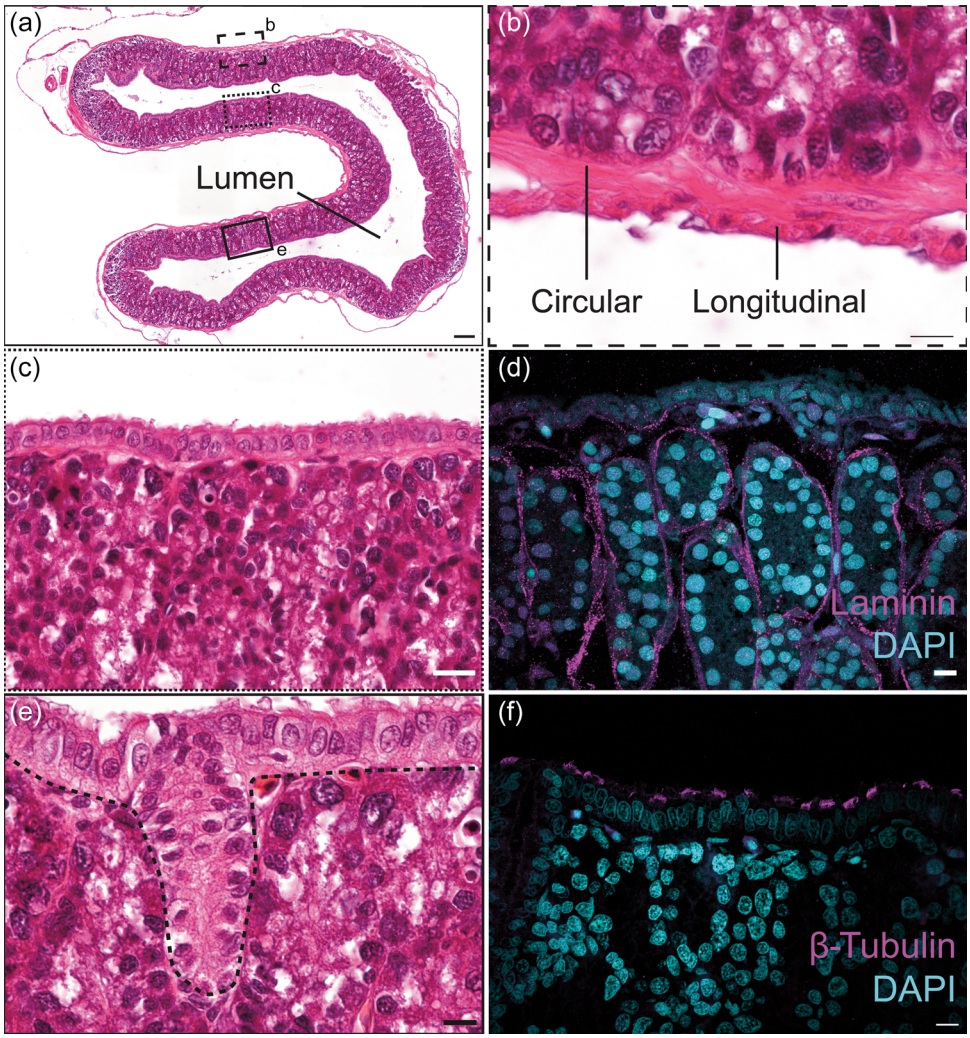

FIGURE 5 (a) Transverse cross-section collected midway through the length of the glandular uterus of a nongravid female. Scale bar = 500 μm. Boxes showing where magnified images were collected are approximate as magnified images were collected from different serial sections. (b, c, e) High-magnification image of glandular uterus cross-section $n = 5$. (d) High magnification image of laminin (magenta) immunofluorescence staining with DAPI (cyan) counterstain of glandular uterus transverse section. (b–f) Scale bar = 10 μm. $n = 3$. Individual from a–c, e, f collected during the breeding season. Individual from (d) collected during the nonbreeding season. In high-magnification images (b–f), lumen is on the top of the image. (f) High magnification image of beta-tubulin (magenta) immunofluorescence staining with DAPI (cyan) counterstain of glandular uterus transverse section.

observed ovulation of follicles from the ovary into the infundibulum, the morphology observed in the anterior infundibulum suggests that it may function like the mammalian infundibulum to receive ovulated oocytes from the ovary. In mammals, the infundibulum is the region of the fallopian tube closest to the ovary. Disruption of cilia formation in the infundibulum and oviduct of mice leads to a failure of oocyte transport into the oviduct after ovulation, implicating cilia as a primary driver of this process (Yuan et al., 2021). Importantly, the infundibulum of mice is structured so that the cilia lining the infundibulum can interact with the ovary in finger-like projections from the infundibulum called fimbriae. These fimbriae are everted so that the inner ciliated epithelium is "outside" at the tip of the infundibulum (Dirksen & Satir, 1972). Because the brown anole phenotype is similar, cilia may also play an important role in oocyte uptake into the reproductive tract, though ovulation is understudied across reptiles.

Differences between the anterior and posterior infundibulum have been described in reptiles. The anterior infundibulum has been described in alligators, lizards, and snakes (Palmer & Guillette Jr, 1992; Sever et al., 2000; Siegel et al., 2014; Siegel & Sever, 2006). The anterior infundibulum has been described as having a highly ciliated epithelium with invaginations into the lamina propria and, in snakes, is described as a site of sperm storage. In cross-section, these data from the literature show a structure similar in morphology to the lip of the infundibulum that we describe here in wholemount, though the invaginations present are described as glands. However, these histological data from the literature do not depict an epithelium that is folded over on itself. The presence of the infundibulum lip in a few species of squamates would suggest that this funnel lip may be present across all squamate reptiles but has yet to be fully described. More detailed whole-mount imaging of the anterior infundibulum in additional squamate reptile species would clarify whether an "inside-out" structure at the anterior infundibulum is convergent between mammals and reptiles or if this is a homologous reproductive feature across tetrapods.

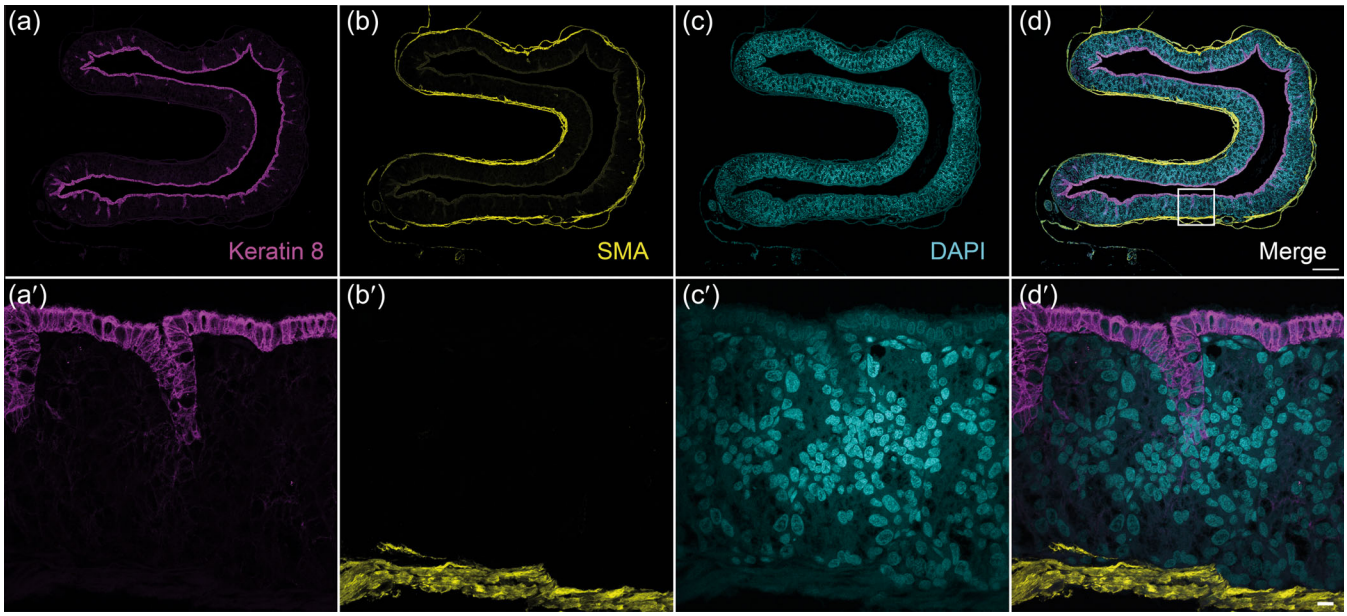

FIGURE 6 Immunohistochemistry of transverse sections of the glandular uterus. (a, a′) Keratin 8 (magenta), (b, b′) smooth muscle actin (yellow), (c, c′) DAPI (cyan), and (d, d′) merged composite antibody staining sections are shown. a–d scale bar = 500 μm, tiled images, a′–d′ scale bar = 50 μm. $n = 3$. Z-step = 3.24 μm, total depth = 12.98 μm for a–d, Z-step = 0.48, total depth = 9.46 μm for a′–d′. In high-magnification images (a′–d′), lumen is on the top of the image. Box showing where magnified images were collected is approximate as magnified images were collected from different serial sections.

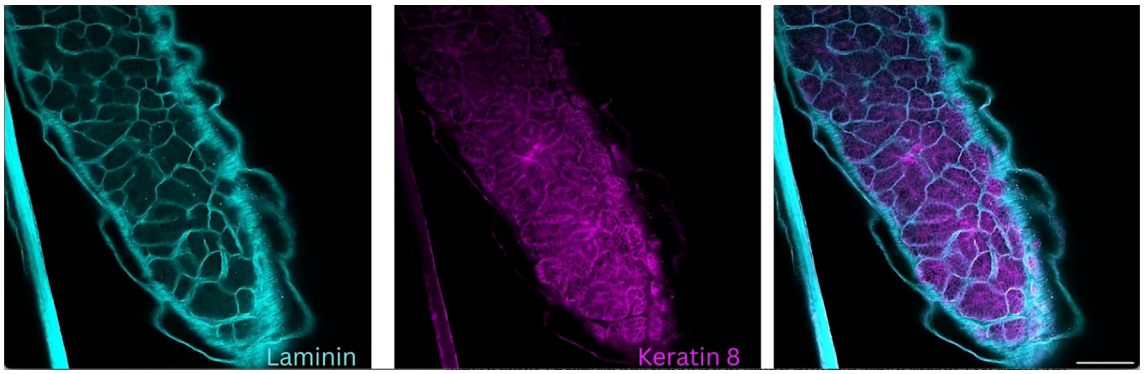

VIDEO 1 Fly-through of optical sections (2.5 μm Z-step, 160 μm total thickness) of whole-mount antibody staining for laminin (cyan) and keratin 8 (magenta). Scale bar = 100 μm. (a) Laminin channel only, (b) keratin 8 channel only, and (c) composite staining. Video content can be viewed at https://onlinelibrary.wiley.com/doi/10.1002/ar.25293

4.2 | Glandular uterus

In the glandular uterus, we have identified two distinct sets of duct-like structures with unique spatial gene expression, one keratin 8 positive set that extends from the epithelium and a second that has an acinar morphology and is surrounded by a laminin-positive basement membrane. The glandular uterus of *Anolis sagrei* is the region of the reproductive tract where the eggshell is deposited, and we show that it is a tubular organ with prominent acinar tissue and prominent epithelial ducts. The morphological features of the *A. sagrei* glandular uterus are very similar to what has been described in the green anole (Noble & Greenberg, 1941), similar to what has been observed in other reptiles (Blackburn, 1998), while the keratin 8 expression we observe in the glandular uterus epithelium is similar to what has been reported in the mammalian uterus. In *Mus musculus* keratin 8 is highly expressed in the epithelial lining of the adult uterus (Magin et al., 1998; Vue & Behringer, 2020). Though uterine morphology varies between mammalian species (Machado et al., 2022), a common feature of the mammalian uterus is the presence of endometrial glands; these glands are present across mammals and secrete

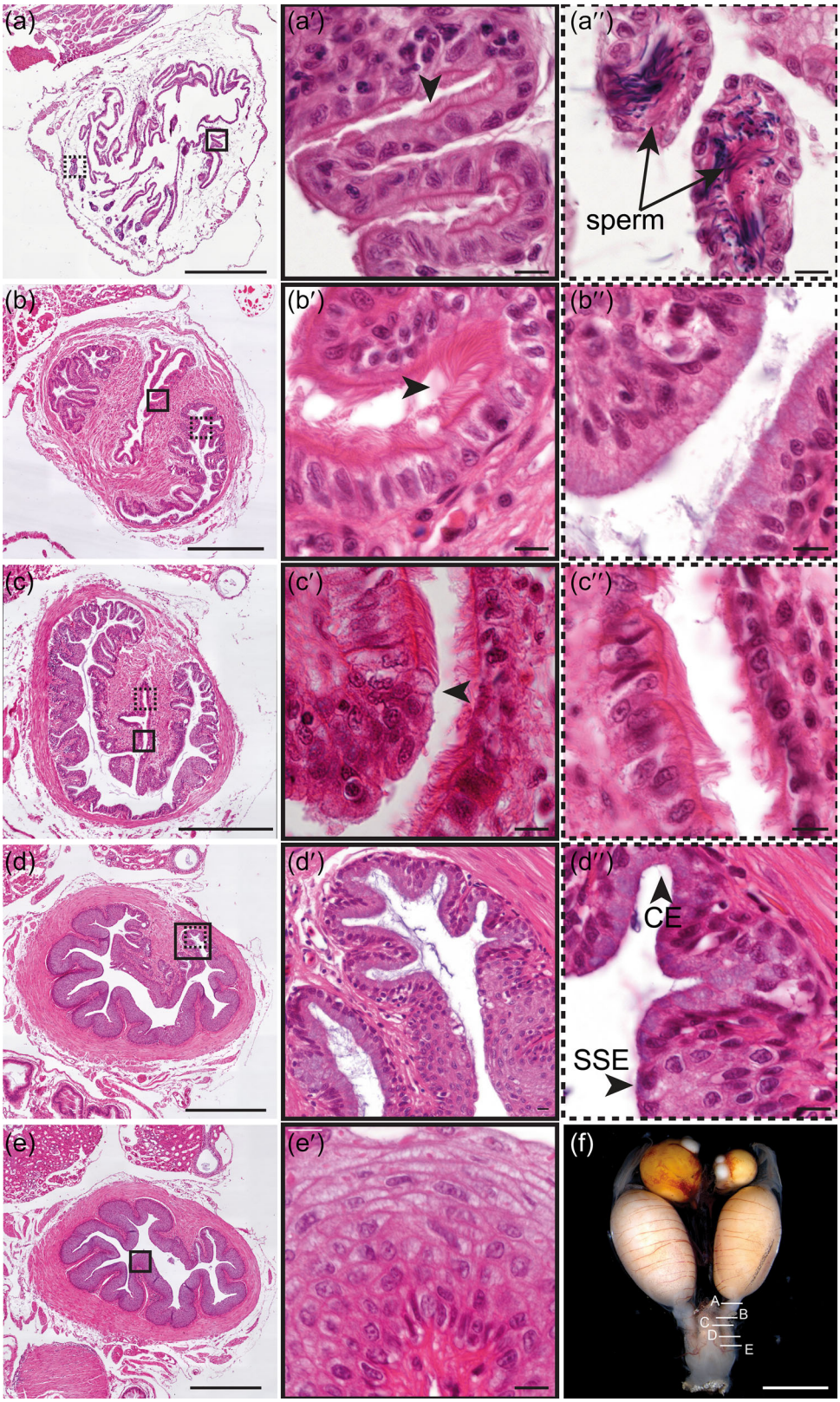

FIGURE 7 Histology of the nonglandular uterus. (a—e) Transverse cross sections progressing from anterior to posterior through the anterior nonglandular uterus. Scale bar = 500 μm. Box with solid outline represents approximately where high-magnification images in a′–e′ were collected. Box with dashed outline represents approximately where high-magnification images in a″–d″ were collected. a′–e′, a″–d″ High-magnification images of features of the nonglandular uterus. Scale bar = 10 μm. Black arrowheads indicate ciliated columnar epithelial cells. $n = 3$. (f) Figure 1b is used to demonstrate approximately where transverse sections were collected. Scale bar = 5 mm. CE, columnar epithelium; SM, smooth muscle; SSE, stratified squamous epithelium.

proteins and substances that are required for embryonic and fetal development (reviewed in Gray et al., 2001). In the mouse, these glands are keratin 8 positive and are present along the length of the uterus, extending from the epithelial lining of the uterine lumen into the surrounding stroma; these glands are dynamic and reoriented towards the site of implantation (Arora et al., 2016). In humans, endometrial glands are also

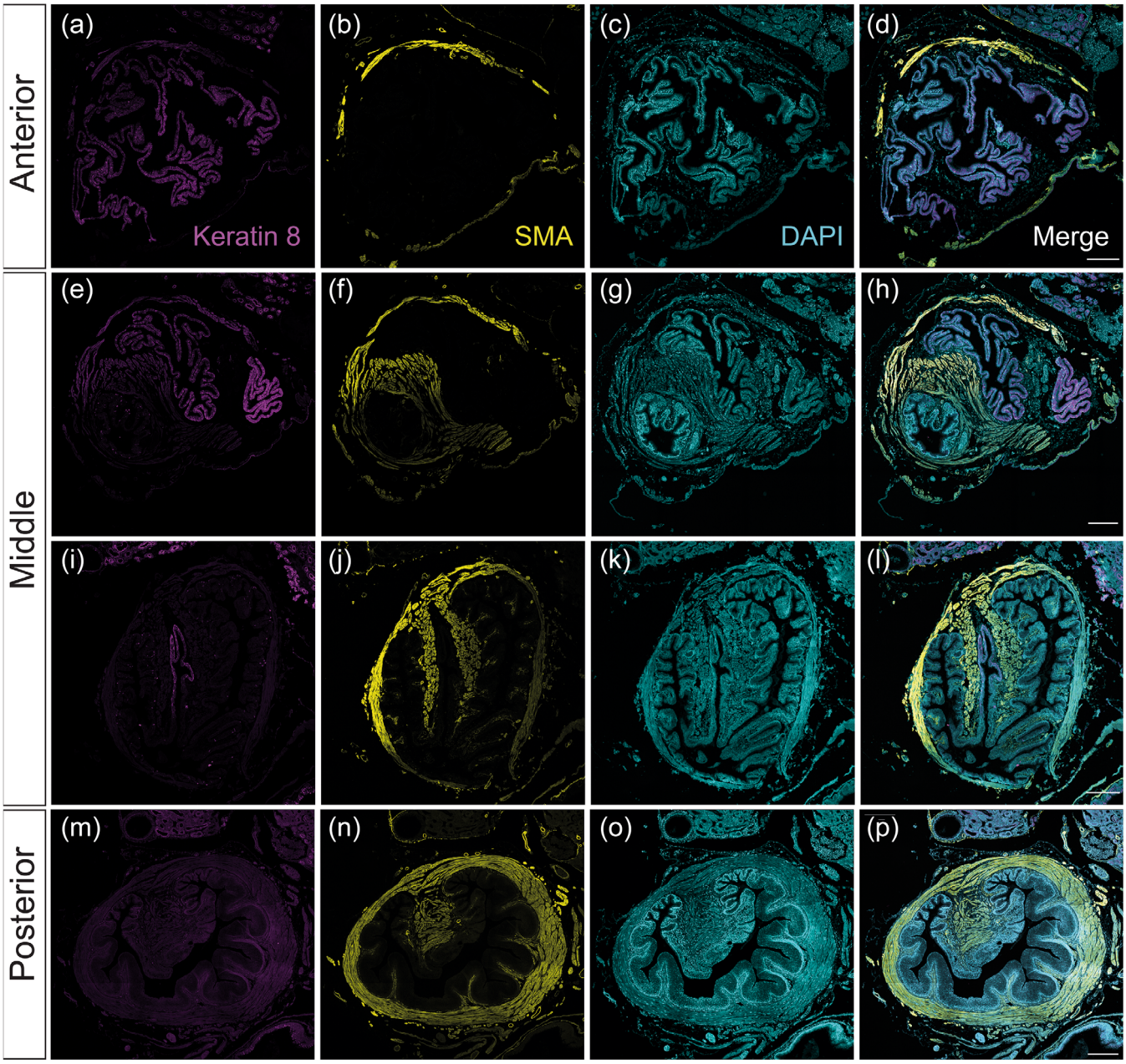

FIGURE 8 Immunohistochemistry of the nonglandular uterus. (a, e, i, m) Keratin 8 (magenta), (b, f, j, n) smooth muscle actin (yellow), (c, g, k, o) DAPI (cyan), and (d, h, l, p) merged antibody staining of transverse cross sections is shown. Scale bar = 200 μm. $n = 3$. For (a–d), Z-step = 2.6 μm, total depth = 10.4 μm; (e–h) Z-step = 2.51 μm, total depth = 12.55 μm; (i–l) Z-step = 2.54 μm, total depth = 12.7 μm; (m–p) Z-step = 0.76 μm, total depth = 12.16 μm.

present (Arora et al., 2016; Yamaguchi et al., 2021). Our data show that the epithelium of the glandular uterus in the brown anole has a different architecture compared to mammalian uterine glands. Though the glands do extend from the epithelium into surrounding tissue and are keratin 8 positive, the glands appear to be less dense across the glandular uterus compared to the mammalian uterus and they appear to be less complex (we did not observe coiling, folding, or budding in the adult glands of *A. sagrei*).

Another difference between the mammalian uterus and the glandular uterus of *A. sagrei* is the presence of a series of acinar structures that are distinct from the keratin 8 positive epithelial ductal structures and defined by the presence of a laminin-positive basement membrane. Though laminins are also expressed in the basement membrane of the endometrial glands of pregnant humans (Yang et al., 2021) and rats (Glasser et al., 1987) as well as pregnant and nonpregnant mice (Jin, 2019; Yang et al., 2021), the acinar structures in the brown

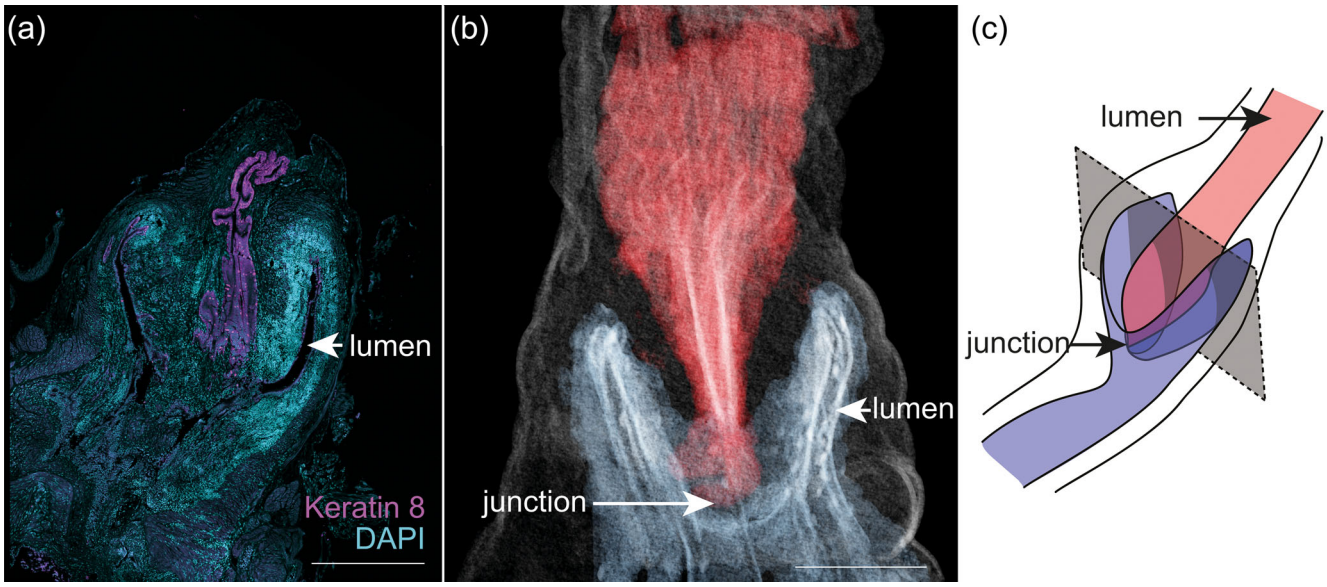

FIGURE 9 (a) Coronal section through the nonglandular uterus showing keratin 8 (magenta) expression and DAPI (cyan) staining. Scale bar = 500 μm. $n = 3$. Z-step = 2.45 μm, total depth = 19.6 μm. (b) Digital segmentation of the epithelium of the nonglandular uterus in ventral view. Tissue reconstructed in red represents the ciliated, simple epithelium, and tissue reconstructed in blue represents the nonciliated simple and nonciliated stratified squamous epithelium. Scale bar = 250 μm. (c) Schematic representation of the nonglandular uterus in medioventral view. Red represents the ciliated, simple epithelium, and blue represents the nonciliated simple and nonciliated stratified squamous epithelium. Gray box with dotted line represents the approximate plane of section of the section from (a).

VIDEO 2 Three-dimensional reconstruction of the entire reproductive tract of the brown anole, highlighting the nonglandular uterus in a phosphotungstic acid-stained specimen. In the highlighted nonglandular uterus, tissue reconstructed in red represents the anterior ciliated, simple epithelium. Tissue reconstructed in blue represents the posterior nonciliated simple and nonciliated stratified squamous epithelium.
Video content can be viewed at https://onlinelibrary.wiley.com/doi/10.1002/ar.25293

anole do not bear much similarity to any of the structures of the mammalian uterus. Instead, they are similar to structures that have been identified in the chicken reproductive tract. Chickens have an organ in which the shell is deposited onto the forming egg called the "uterus" or the "shell gland." The eggshell is deposited here (Nys & Guyot, 2011) and this is accomplished in part by transfer of calcium from the bloodstream to a secreted fluid that facilitates calcification of the shell around the developing egg (Vetter & O'Grady, 2005). The glands of this organ are similarly structured with an acinar morphology and small lumen; there is also a laminin-positive basement membrane surrounding these glands, similar to that observed here in *A. sagrei* (Madekurozwa, 2013), suggesting that the acinar structures we observe here may play a role in shell deposition in lizards. In the oviparous skink *Lampropholis guichenoti*, gland-like structures in the glandular uterus stain strongly for Ca^{2+}ATPase pumps during the breeding season, suggesting that calcification of the eggshell is mediated by these structures (Herbert et al., 2006). Ultimately, further study of the role of the duct-like tissue in the glandular uterus of *A. sagrei* is required.

4.3 | Nonglandular uterus

By examining the morphological and gene expression changes from anterior to posterior in the nonglandular uterus we identified two distinct regions which correspond to the mammalian cervix and vagina. We have examined the three-dimensional morphology of the nonglandular uterus through a combination of 2D histology and CT volumetric analysis. In both the CT and histological transverse cross-sections, we observe anteriorly, a

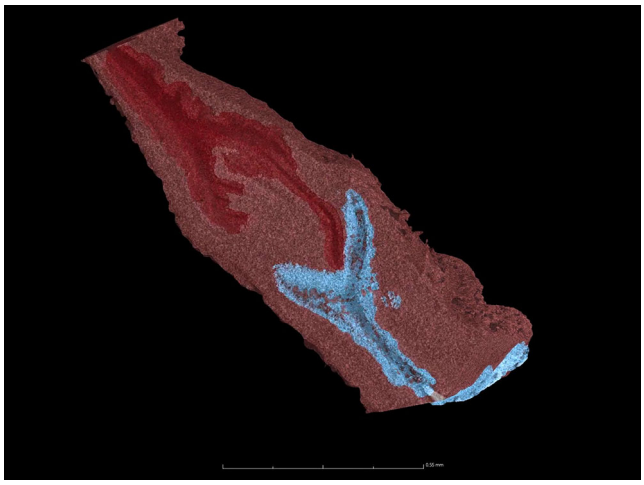

VIDEO 3 Three-dimensional reconstruction of a single nonglandular uterus in a diceCT *A. sagrei* scan. Tissue reconstructed in maroon represents nonepithelial tissue in the nonglandular uterus. Tissue reconstructed in red represents the ciliated, simple epithelium, and blue represents the nonciliated simple and nonciliated stratified squamous epithelium. The first fly-through represents a sagittal plane of section. The second fly-through represents a coronal plane of section moving from ventral to dorsal. The third fly-through represents a transverse plane of section moving from anterior to posterior.
Video content can be viewed at https://onlinelibrary.wiley.com/doi/10.1002/ar.25293

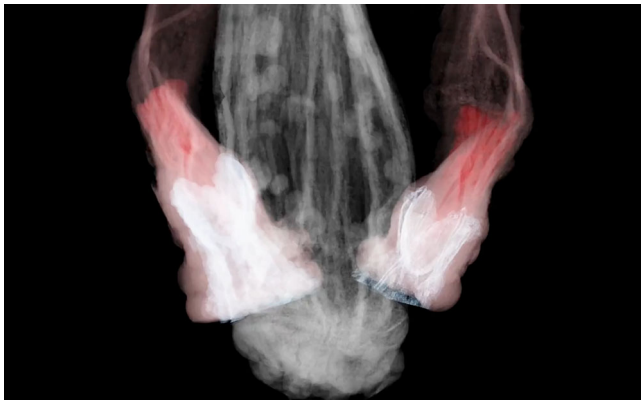

VIDEO 4 Three-dimensional reconstruction of both left and right nonglandular uteruses with the digestive tract in between from a diceCT *A. sagrei* scan. Tissue digitally reconstructed in white represented the digestive tract. Tissue reconstructed in pink represents the outside of the nonglandular uterus. Tissue reconstructed in red represents the ciliated, simple epithelium, and blue represents the nonciliated simple and nonciliated stratified squamous epithelium.
Video content can be viewed at https://onlinelibrary.wiley.com/doi/10.1002/ar.25293

single lumen surrounded by a highly folded epithelium in the brown anole, and posteriorly, three distinct lumens in cross-section. The central, ciliated lumen is bracketed

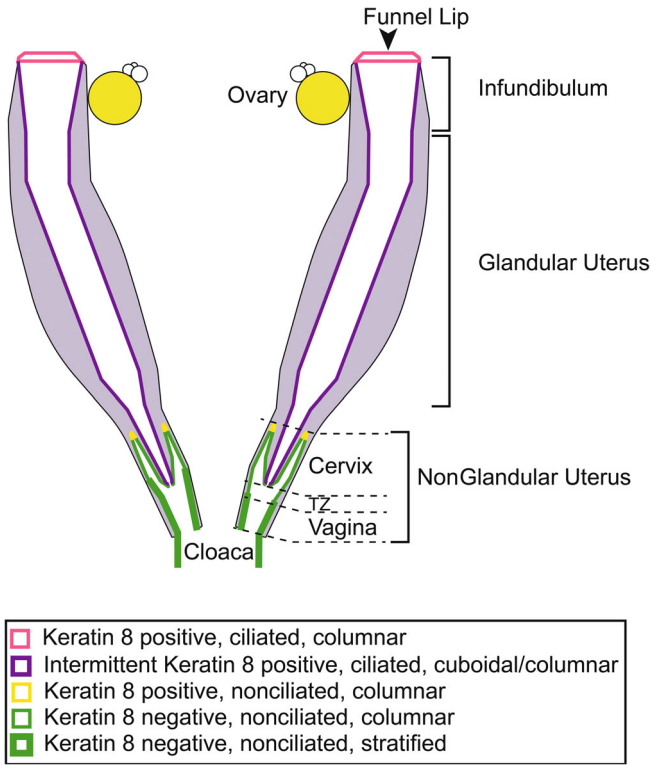

FIGURE 10 Model depicting the data collected in this study. Differences in the morphology and gene expression of the epithelium are summarized by changes to the line thickness and line color across the reproductive tract.

by two lateral, unciliated lumen which represent the anterior horns of the cupula. More posteriorly, these three lumens merge into one before meeting the intestines at the cloaca. Similar cross-sectional patterns of lumen have been reported in the nonglandular uterus of the green anole (Noble & Greenberg, 1941) and in the cervix of the mouse (Forsberg, 1969). We generated a 3D reconstruction of the nonglandular uterus lumen using micro-CT analysis and reveal a series of internal folds within the nonglandular uterus congruent with the two-dimensional data. By combining 2D and 3D methodologies, we are able to show that the nonglandular uterus is a complex and heterogeneous organ that is morphologically similar to the mammalian cervix and vagina (Chumduri et al., 2021).

We present further support for the presence of the lizard cervix by showing that cellular architecture and gene expression changes across the nonglandular uterus are similar to those seen in mammals. We show a transition from simple columnar epithelium to stratified squamous epithelium which mimics the transition from the mammalian uterus to the vagina in the cervix. The anterior nonglandular uterus of the brown anole has a folded, cuboidal/columnar, ciliated, keratin 8 positive epithelium

that transitions into a keratin 8 negative, nonciliated, stratified epithelium more posteriorly. This epithelial transition is accompanied by a separation of the central anterior lumen into three distinct lumens that are joined posteriorly. Antibody staining against keratin 8 in mice has shown a similar loss of epithelial keratin 8 expression moving from anterior (simple epithelium) to posterior (stratified epithelium) through the cervix (Chumduri et al., 2021). Given these similarities, we recommend that the posterior nonglandular uterus (stratified epithelium, keratin 8 negative) be termed the vagina while the anterior nonglandular uterus (simple epithelium and both keratin 8 positive/negative) be termed the cervix (Figure 10). We also define a transition zone where the keratin 8 negative epithelium transitions from simple to stratified moving anterior to posterior (Figures 7d and 10). We recommend maintaining the classification of the two regions together as the nonglandular uterus. Currently, many of the morphological descriptions of the reptilian reproductive tract classify the nonglandular uterus as a single organ. However, our data suggest that the singular classification of the nonglandular uterus overlooks the histology and gene expression of the system and that a separate morphological classification of the anterior and posterior nonglandular uterus would be more accurate and useful. We believe that continued use of the term "nonglandular uterus" will be important for cohesion in the literature but that additional use of the term "cervix" can help clarify the morphological changes from anterior to posterior in the nonglandular uterus.

Though we have observed these similarities, there are differences between the reptilian and mammalian cervix. Humans have both secretory and ciliated cells lining the cervical lumen (Hafez, 1982) while in mice, the cervix does not have cilia on any of the epithelial cells lining the cervical lumen (Lamb et al., 1978). In the brown anole, we find cilia throughout the anterior nonglandular uterus. Though the presence of cilia in the reproductive tract in other species is known to facilitate embryo and sperm movement, the function of the cilia in the *A. sagrei* nonglandular uterus and cervix remains unclear. Our data also show that the transition from simple to stratified epithelium and associated loss of epithelial keratin 8 expression seen in the mouse cervix (Chumduri et al., 2021) is not identical in the brown anole. Instead, we see that keratin 8 expression occurs slightly anterior to the transition from stratified to simple epithelium, meaning that there are some simple epithelial cells in the nonglandular uterus that are keratin 8 negative, and that the most anterior portions of the nonciliated lumen are keratin 8 positive. Thus, despite the similarities between the anole and mammalian cervix, there appear to be species specific changes in morphology and gene expression that need to be further characterized.

The same cervix morphology distinctions seen here in *A. sagrei* are also observed in *Anolis carolinensis* (Noble & Greenberg, 1941) though it is not described as such. In the snake *Toluca lineata*, an "oviductal-cloacal transition" is described and the morphology looks very similar to that described above (Uribe et al., 1998). Stratified epithelium in the reptilian reproductive system has been reported to be "rare" (Blackburn, 1998). However, comprehensive morphological examination of the reptilian reproductive system is also rare. A functional cervix has been described in reptiles as the lower portion of the reproductive tract that prevents the fertilized egg from leaving the glandular uterus (Guillette Jr et al., 1991) but this review did not report the morphology of this region. Future study of the reptilian reproductive tract would benefit from detailed histological examination of the nonglandular uterus as well as expression of keratin 8 or other markers of ciliated, simple epithelium. However, in mice, a subpopulation of cervical epithelia cells expresses the simple epithelial marker keratin 8 along with a marker of squamous epithelium keratin 5, indicating that there are cells that could transdifferentiate between keratin 8 positive and keratin 5 positive identities (Cooley et al., 2023). This implies that keratin 8 expression alone is insufficient as a marker to fully understand the tissue composition in the nonglandular uterus and that a suite of markers would provide more comprehensive information. In mice, WT1 expression is restricted to the distal oviduct while PAX2 is expressed in the proximal oviduct (Ford et al., 2021). FOXA2 is a marker of endometrial glands in the mouse uterus (Besnard et al., 2004) and in humans, a suite of markers including various keratins, steroid hormone receptors, and hox genes has been shown to have tissue- and stage-specific expression (Cunha et al., 2017). Testing the expression of published tissue-specific markers in reptiles may further clarify the general tissue architecture as well as potentially homologous structures of the tetrapod reproductive tract. We believe it is likely that the reptilian cervix is more ubiquitous than has been described in the literature. Resources such as MorphoSource provide easily available contrast-enhanced microCT data sets, making our ability to search for morphological variation across reptiles easier than ever before.

The function of the nonglandular uterus so far remains poorly understood. Most commonly, the nonglandular uterus is reported as a site for sperm storage in reptiles (Sever & Hamlett, 2002) and we did observe sperm in the nonglandular uterus, restricted to the anterior region, immediately posterior to the glandular uterus. However, it seems likely that the nonglandular

uterus plays additional important roles in the reproduction of the brown anole. In mammals, the cervix serves to retain the conceptus during pregnancy and act as a barrier to infection by generation of a mucosal plug (Nott et al., 2016). There is extensive remodeling of the cervix during mammalian pregnancy known to be partially regulated by precise timing in hormonal fluctuations (Cooley et al., 2023; Timmons et al., 2010). It is highly likely that functionally similar processes occur in lizards as ovarian follicles are ovulated every 10–14 days and fertilized eggs are retained for a precise amount of time in the glandular uterus before laying (Crews, 1980). Also, the three-dimensional morphology of the nonglandular uterus may hint at a functional role for this organ in egg retention. In the cervix of the nonglandular uterus, the central junction is highly muscled and the lumen is almost completely closed. At this same point, there is a kink in the lumen, that may block passage through the tube. These features could serve as a functional barrier between the fertilized egg in the glandular uterus and the cloaca. Future work examining cervical changes before, during, and after gravidity will further clarify the role of the nonglandular uterus during brown anole reproduction.

4.4 | Homology, function, and development

Despite the morphological, gene expression, and possible functional similarities between the mammalian systems and *A. sagrei*, it is challenging to draw conclusions about homology of the uterine organs between these two groups. An unbiased examination and comparison of gene expression would strengthen our ability to answer questions about the evolution of the tetrapod reproductive system. Questions about homology can also be addressed by examining the development of adult structures; shared developmental trajectories can suggest a shared evolutionary history even with morphological differences between adults. However, both reptiles and mammals exhibit a wide array of reproductive strategies, offspring number, and reproductive tract morphology (Machado et al., 2022; Meiri et al., 2020). More work examining the architecture of the reproductive system in many diverse species will deepen our ability to understand the evolution of the reproductive system across vertebrates.

AUTHOR CONTRIBUTIONS

Bonnie K. Kircher: Conceptualization; investigation; writing – original draft; methodology; visualization; writing – review and editing; data curation; funding acquisition. **Edward L. Stanley:** Investigation; methodology; writing – review and editing; visualization; data curation. **Richard R. Behringer:** Conceptualization; funding acquisition; writing – review and editing; methodology; project administration; resources; supervision; data curation; investigation.

ACKNOWLEDGMENTS

The authors thank the Behringer lab members for helpful comments on the manuscript, Dr Adriana Paulucci-Holthauzen for confocal microscope training and advice, Dr Martin Cohn for his support and enthusiasm, and Dr Stephen Benigno and the Houston Arboretum for facilitating animal collection. This research was supported by National Institutes of Health (NIH) grant HD30284 and the Ben F. Love Endowment to Richard R. Behringer. Bonnie K. Kircher was supported by NIH T32HD098068 and a National Science Foundation (NSF) Postdoctoral Research Fellowship in Biology (PRFB), Division of Biological Infrastructure (DBI) 2209150. Confocal microscopy was supported by NIH shared instrumentation grant OD024976. MicroCT scanning was supported by NSF Division of Materials Reasearch (DMR) grant number 2017977. Veterinary resources were supported by NIH grant CA16672.

ORCID

Bonnie K. Kircher https://orcid.org/0000-0002-9469-575X

Edward L. Stanley https://orcid.org/0000-0001-5257-037X

Richard R. Behringer https://orcid.org/0000-0001-7282-1543

REFERENCES

Abe, T., Kaneko, M., & Kiyonari, H. (2023). A reverse genetic approach in geckos with the CRISPR/Cas9 system by oocyte microinjection. *Developmental Biology*, *497*, 26–32.

Adams, S., Hosie, M., Murphy, C., & Thompson, M. (2004). Changes in oviductal morphology of the skink, *Lampropholis guichenoti*, associated with egg production. *Journal of Morphology*, *262*, 536–544.

Adams, S. M., Lui, S., Jones, S. M., Thompson, M. B., & Murphy, C. R. (2007). Uterine epithelial changes during placentation in the viviparous skink *Eulamprus tympanum*. *Journal of Morphology*, *268*, 385–400.

Arora, R., Fries, A., Oelerich, K., Marchuk, K., Sabeur, K., Giudice, L. C., & Laird, D. J. (2016). Insights from imaging the implanting embryo and the uterine environment in three dimensions. *Development*, *143*, 4749–4754.

Bassi, E. A., de Oliveira, C., Braz, H. B., & de Almeida-Santos, S. M. (2018). How does oocyte uptake occur? A macroscopic study of the ovarian and oviductal modifications for egg capture in the coral-snake *Micrurus corallinus*. *The Anatomical Record*, *301*, 1936–1943.

Besnard, V., Wert, S. E., Hull, W. M., & Whitsett, J. A. (2004). Immunohistochemical localization of Foxa1 and Foxa2 in mouse embryos and adult tissues. *Gene Expression Patterns*, *5*, 193–208.

Biazik, J. M., Thompson, M. B., & Murphy, C. R. (2008). Claudin-5 is restricted to the tight junction region of uterine epithelial cells in the uterus of pregnant/gravid squamate reptiles. *The Anatomical Record: Advances in Integrative Anatomy and Evolutionary Biology*, *291*, 547–556.

Biazik, J. M., Thompson, M. B., & Murphy, C. R. (2009). Lysosomal and alkaline phosphatase activity indicate macromolecule transport across the uterine epithelium in two viviparous skinks with complex placenta. *Journal of Experimental Zoology Part B: Molecular and Developmental Evolution*, *312*, 817–826.

Blackburn, D. G. (1998). Structure, function, and evolution of the oviducts of squamate reptiles, with special reference to viviparity and placentation. *The Journal of Experimental Biology*, *282*, 560–617.

Blackburn, D. G. (1999). Are viviparity and egg-guarding evolutionarily labile in squamates? *Herpetologica*, *55*, 556–573.

Blackburn, D. G. (2015). Evolution of vertebrate viviparity and specializations for fetal nutrition: A quantitative and qualitative analysis. *Journal of Morphology*, *276*, 961–990.

Chumduri, C., Gurumurthy, R. K., Berger, H., Dietrich, O., Kumar, N., Koster, S., Brinkmann, V., Hoffmann, K., Drabkina, M., & Arampatzi, P. (2021). Opposing Wnt signals regulate cervical squamocolumnar homeostasis and emergence of metaplasia. *Nature Cell Biology*, *23*, 184–197.

Conner, J., & Crews, D. (1980). Sperm transfer and storage in the lizard, *Anolis carolinensis*. *Journal of Morphology*, *163*, 331–348.

Conroy, C., Papenfuss, T., Parker, J., & Hahn, N. (2009). Use of tricaine methanesulfonate (MS222) for euthanasia of reptiles. *Journal of the American Association for Laboratory Animal Science*, *48*, 28–32.

Cooley, A., Madhukaran, S., Stroebele, E., Caraballo, M. C., Wang, L., Akgul, Y., Hon, G. C., & Mahendroo, M. (2023). Dynamic states of cervical epithelia during pregnancy and epithelial barrier disruption. *iScience*, *26*, 105953.

Crews, D. (1977). The annotated anole: Studies on control of lizard reproduction: Anoline lizards make excellent experimental animals for analyzing reproduction at the physiological, behavioral, and species levels. *American Scientist*, *65*, 428–434.

Crews, D. (1980). Interrelationships among ecological, behavioral, and neuroendocrine processes in the reproductive cycle of Anolis carolinensis and other reptiles. In *Advances in the study of behavior* (pp. 1–74). Elsevier.

Crow, J., Amso, N. N., Lewin, J., & Shaw, R. W. (1994). Physiology: Morphology and ultrastructure of fallopian tube epithelium at different stages of the menstrual cycle and menopause. *Human Reproduction*, *9*, 2224–2233.

Cuellar, O. (1970). Egg transport in lizards. *Journal of Morphology*, *130*, 129–135.

Cunha, G. R., Kurita, T., Cao, M., Shen, J., Robboy, S., & Baskin, L. (2017). Molecular mechanisms of development of the human fetal female reproductive tract. *Differentiation*, *97*, 54–72.

Dirksen, E. R., & Satir, P. (1972). Ciliary activity in the mouse oviduct as studied by transmission and scanning electron microscopy. *Tissue and Cell*, *4*, 389–403.

Evans, L. T., & Clapp, M. L. (1940). The effects of ovarian hormones and seasons on *Anolis carolinensis*. II. The genital system. *The Anatomical Record*, *77*, 57–75.

Ford, M. J., Harwalkar, K., Pacis, A. S., Maunsell, H., Wang, Y. C., Badescu, D., Teng, K., Yamanaka, N., Bouchard, M., & Ragoussis, J. (2021). Oviduct epithelial cells constitute two developmentally distinct lineages that are spatially separated along the distal-proximal axis. *Cell Reports*, *36*, 109677.

Forsberg, J.-G. (1969). The development of atypical epithelium in the mouse uterine cervix and vaginal fornix after neonatal oestradiol treatment. *British Journal of Experimental Pathology*, *50*, 187.

Fox, W. (1963). Special tubules for sperm storage in female lizards. *Nature*, *198*, 500–501.

Fox, W., & Dessauer, H. C. (1962). The single right oviduct and other urogenital structures of female *Typhlops* and *Leptotyphlops*. *Copeia*, *1962*, 590–597.

Gabe, M., & Saint Girons, H. (1965). *Contribution a la morphologie comparee du cloaque et des glandes epidermoides de la region cloacale chez les lepidosauriens*. Éditions du Muséum.

Garcia-Elfring, A., Sabin, C. E., Iouchmanov, A. L., Roffey, H. L., Samudra, S. P., Alcala, A. J., Osman, R. S., Lauderdale, J. D., Hendry, A. P., & Menke, D. B. (2023). Piebaldism and chromatophore development in reptiles is linked to the TFEC gene. *Current Biology*, *33*(4), 755–763.e3.

Geneva, A. J., Park, S., Bock, D. G., de Mello, P. L., Sarigol, F., Tollis, M., Donihue, C. M., Reynolds, R. G., Feiner, N., & Rasys, A. M. (2022). Chromosome-scale genome assembly of the brown anole (*Anolis sagrei*), an emerging model species. *Communications Biology*, *5*, 1–13.

Gignac, P. M., Kley, N. J., Clarke, J. A., Colbert, M. W., Morhardt, A. C., Cerio, D., Cost, I. N., Cox, P. G., Daza, J. D., & Early, C. M. (2016). Diffusible iodine-based contrast-enhanced computed tomography (diceCT): An emerging tool for rapid, high-resolution, 3-D imaging of metazoan soft tissues. *Journal of Anatomy*, *228*, 889–909.

Girling, J., Cree, A., & Guillette, L. J., Jr. (1997). Oviductal structure in a viviparous New Zealand gecko, *Hoplodactylus maculatus*. *Journal of Morphology*, *234*, 51–68.

Girling, J., Guillette, L., Jr., & Cree, A. (2000). Ultrastructure of the uterus in an ovariectomized gecko (*Hemidactylus turcicus*) after administration of exogenous estradiol. *The Journal of Experimental Zoology*, *286*, 76–89.

Girling, J. E. (2002). The reptilian oviduct: A review of structure and function and directions for future research. *The Journal of Experimental Zoology*, *293*, 141–170.

Glasser, S. R., Lampelo, S., Munir, M. I., & Julian, J. (1987). Expression of desmin, laminin and fibronectin during in situ differentiation (decidualization) of rat uterine stromal cells. *Differentiation*, *35*, 132–142.

Gray, C. A., Bartol, F. F., Tarleton, B. J., Wiley, A. A., Johnson, G. A., Bazer, F. W., & Spencer, T. E. (2001). Developmental biology of uterine glands. *Biology of Reproduction*, *65*, 1311–1323.

Guillette, L., Jr., Dubois, D. H., & Cree, A. (1991). Prostaglandins, oviducal function, and parturient behavior in nonmammalian vertebrates. *American Journal of Physiology. Regulatory, Integrative and Comparative Physiology*, *260*, R854–R861.

Hafez, E. (1982). Structural and ultrastructural parameters of the uterine cervix. *Obstetrical & Gynecological Survey*, *37*, 507–516.

Hama, H., Hioki, H., Namiki, K., Hoshida, T., Kurokawa, H., Ishidate, F., Kaneko, T., Akagi, T., Saito, T., & Saido, T. (2015). Scale*S*: An optical clearing palette for biological imaging. *Nature Neuroscience*, *18*, 1518–1529.

Herbert, J. F., Lindsay, L. A., Murphy, C. R., & Thompson, M. B. (2006). Calcium transport across the uterine epithelium of pregnant lizards. *Herpetological Monographs*, *20*, 205–211.

Jin, S. (2019). Bipotent stem cells support the cyclical regeneration of endometrial epithelium of the murine uterus. *Proceedings of the National Academy of Sciences of the United States of America*, *116*, 6848–6857.

Lamb, J. C., IV, Newbold, R., Stumpf, W. E., & McLachlan, J. (1978). Transitional changes in the surface epithelium of the cycling mouse vagina, cervix and uterus: Scanning electron microscopic studies. *Biology of Reproduction*, *19*, 701–711.

Lesciotto, K. M., Motch Perrine, S. M., Kawasaki, M., Stecko, T., Ryan, T. M., Kawasaki, K., & Richtsmeier, J. T. (2020). Phosphotungstic acid-enhanced microCT: Optimized protocols for embryonic and early postnatal mice. *Developmental Dynamics*, *249*, 573–585.

Losos, J. B. (2009). *Lizards in an evolutionary tree*. University of California Press.

Lovern, M. B., Holmes, M. M., & Wade, J. (2004). The green anole (Anolis). *Institute for Laboratory Animal Research Journal*, *45*, 54–64.

Machado, D. A., Ontiveros, A. E., & Behringer, R. R. (2022). Mammalian uterine morphogenesis and variations. In T. Gridley & L. Oxburgh (Eds.), *Mouse models of development and disease* (pp. 52–77). Academic Press.

Madekurozwa, M. C. (2013). An immunohistochemical study of the oviduct in the domestic fowl (*Gallus domesticus*). *Anatomia, Histologia, Embryologia*, *42*, 48–56.

Magin, T. M., Schröder, R., Leitgeb, S., Wanninger, F., Zatloukal, K., Grund, C., & Melton, D. W. (1998). Lessons from keratin 18 knockout mice: Formation of novel keratin filaments, secondary loss of keratin 7 and accumulation of liver-specific keratin 8-positive aggregates. *The Journal of Cell Biology*, *140*, 1441–1451.

Meiri, S., Avila, L., Bauer, A. M., Chapple, D. G., Das, I., Doan, T. M., Doughty, P., Ellis, R., Grismer, L., & Kraus, F. (2020). The global diversity and distribution of lizard clutch sizes. *Global Ecology and Biogeography*, *29*, 1515–1530.

Murphy, B. F., Parker, S. L., Murphy, C. R., & Thompson, M. B. (2011). Placentation in the eastern water skink (*Eulamprus quoyii*): A placentome-like structure in a lecithotrophic lizard. *Journal of Anatomy*, *218*, 678–689.

Noble, G. K., & Greenberg, B. (1941). Effects of seasons, castration and crystalline sex hormones upon the urogenital system and sexual behavior of the lizard (*Anolis carolinensis*). I. The adult female. *Journal of Experimental Zoology*, *88*, 451–479.

Nogueira, K. O. P. C., Rodrigues, S. S., Araújo, V. A., & Neves, C. A. (2011). Oviductal structure and ultrastructure of the oviparous gecko, *Hemidactylus mabouia* (Moreau De Jonnès, 1818). *The Anatomical Record: Advances in Integrative Anatomy and Evolutionary Biology*, *294*, 883–892.

Nott, J. P., Bonney, E. A., Pickering, J. D., & Simpson, N. A. (2016). The structure and function of the cervix during pregnancy. *Translational Research in Anatomy*, *2*, 1–7.

Nys, Y., & Guyot, N. (2011). Egg formation and chemistry. In *Improving the safety and quality of eggs and egg products* (pp. 83–132). Woodhead Publishing.

Ortiz, E., & Morales, M. H. (1974). Development and function of the female reproductive tract of the tropical lizard, *Anolis pulchellus*. *Physiological Zoology*, *47*, 207–217.

Palmer, B. D., & Guillette, L. J., Jr. (1992). Alligators provide evidence for the evolution of an archosaurian mode of oviparity. *Biology of Reproduction*, *46*, 39–47.

Parker, S. L., Manconi, F., Murphy, C. R., & Thompson, M. B. (2010). Uterine and placental angiogenesis in the Australian skinks, *Ctenotus taeniolatus*, and *Saiphos equalis*. *The Anatomical Record: Advances in Integrative Anatomy and Evolutionary Biology*, *293*, 829–838.

Rasys, A. M., Park, S., Ball, R. E., Alcala, A. J., Lauderdale, J. D., & Menke, D. B. (2019). CRISPR-Cas9 gene editing in lizards through microinjection of unfertilized oocytes. *Cell Reports*, *28*, 2288–2292.e2283.

Rojas, C. A., Barros, V. A., & Almeida-Santos, S. M. (2019). A histological and ultrastructural investigation of the female reproductive system of the water snake (*Erythrolamprus miliaris*): Oviductal cycle and sperm storage. *Acta Zoologica*, *100*, 69–80.

Sanger, T. J., Hime, P. M., Johnson, M. A., Diani, J., & Losos, J. B. (2008). Laboratory protocols for husbandry and embryo collection of *Anolis* lizards. *Herpetological Review*, *39*, 58–63.

Sanger, T. J., & Kircher, B. K. (2017). Model clades versus model species: Anolis lizards as an integrative model of anatomical evolution. *Methods in Molecular Biology (Clifton, N.J.)*, *1650*, 285–297.

Schindelin, J., Arganda-Carreras, I., Frise, E., Kaynig, V., Longair, M., Pietzsch, T., Preibisch, S., Rueden, C., Saalfeld, S., & Schmid, B. (2012). Fiji: An open-source platform for biological-image analysis. *Nature Methods*, *9*, 676–682.

Sever, D. M., & Hamlett, W. C. (2002). Female sperm storage in reptiles. *The Journal of Experimental Zoology*, *292*, 187–199.

Sever, D. M., Ryan, T. J., Morris, T., Patton, D., & Swafford, S. (2000). Ultrastructure of the reproductive system of the black swamp snake (*Seminatrix pygaea*). II. Annual oviducal cycle. *Journal of Morphology*, *245*, 146–160.

Siegel, D. S., Miralles, A., Rheubert, J. L., & Sever, D. M. (2014). Female reproductive anatomy: Cloaca, oviduct, and sperm storage. In J. L. Rheubert, D. S. Siegel, & S. E. Trauth (Eds.), *Reproductive biology and phylogeny of lizards and tuatara*. CRC Press.

Siegel, D. S., & Sever, D. M. (2006). Utero-muscular twisting and sperm storage in viperids. *Herpetological Conservation and Biology*, *1*, 87–92.

Thompson, M. B., Biazik, J. B., Lui, S., Adams, S. M., & Murphy, C. R. (2006). Morphological and functional changes to the uterus of lizards with different placental complexities. *Herpetological Monographs*, *20*, 178–185.

Timmons, B., Akins, M., & Mahendroo, M. (2010). Cervical remodeling during pregnancy and parturition. *Trends in Endocrinology and Metabolism*, *21*, 353–361.

Tinkle, D. W., & Gibbons, J. W. (1977). *The distribution and evolution of viviparity in reptiles*. University of Michigan.

Uribe, M. C., González-Porter, G., Palmer, B. D., & Guillette, L. J., Jr. (1998). Cyclic histological changes of the oviductal-cloacal junction in the viviparous snake *Toluca lineata*. *Journal of Morphology*, *237*, 91–100.

Vetter, A. E., & O'Grady, S. M. (2005). Sodium and anion transport across the avian uterine (shell gland) epithelium. *The Journal of Experimental Biology*, *208*, 479–486.

Vue, Z., & Behringer, R. R. (2020). Epithelial morphogenesis in the perinatal mouse uterus. *Developmental Dynamics*, *249*, 1377–1386.

Wu, Q., Thompson, M. B., & Murphy, C. R. (2011). Changing distribution of cadherins during gestation in the uterine epithelium of lizards. *Journal of Experimental Zoology Part B: Molecular and Developmental Evolution*, *316*, 440–450.

Yamaguchi, M., Yoshihara, K., Suda, K., Nakaoka, H., Yachida, N., Ueda, H., Sugino, K., Mori, Y., Yamawaki, K., & Tamura, R. (2021). Three-dimensional understanding of the morphological complexity of the human uterine endometrium. *iScience*, *24*, 102258.

Yang, Z.-S., Pan, H.-Y., Shi, W.-W., Chen, S.-T., Wang, Y., Li, M.-Y., Zhang, H.-Y., Yang, C., Liu, A.-X., & Yang, Z.-M. (2021). Regulation and function of laminin A5 during mouse and human decidualization. *International Journal of Molecular Sciences*, *23*, 199.

Yuan, S., Wang, Z., Peng, H., Ward, S. M., Hennig, G. W., Zheng, H., & Yan, W. (2021). Oviductal motile cilia are essential for oocyte pickup but dispensable for sperm and embryo transport. *Proceedings of the National Academy of Sciences of the United States of America*, *118*, e2102940118.

SUPPORTING INFORMATION

Additional supporting information can be found online in the Supporting Information section at the end of this article.

How to cite this article: Kircher, B. K., Stanley, E. L., & Behringer, R. R. (2023). Anatomy of the female reproductive tract organs of the brown anole (*Anolis sagrei*). *The Anatomical Record*, 1–19. https://doi.org/10.1002/ar.25293